

**EFFECT OF INDIUM DOPING ON  
STRUCTURAL, OPTICAL AND ELECTRICAL  
PROPERTIES OF ZINC OXIDE THIN FILMS**

**NORNANI BINTI MD AZNAN**

**UNIVERSITI SAINS MALAYSIA**

**2016**

**EFFECT OF INDIUM DOPING ON  
STRUCTURAL, OPTICAL AND ELECTRICAL  
PROPERTIES OF ZINC OXIDE THIN FILMS**

**by**

**NORNANI BINTI MD AZNAN**

**Thesis submitted in fulfilment of the requirements  
for the degree of  
Master of Science**

**August 2016**

## **ACKNOWLEDGEMENT**

I would like to express my greatest gratitude to Allah S.W.T. for giving me the strength and ease my path to complete this thesis. Alhamdulillah. To accomplish a goal, hard work alone is not enough. The help and support from others are equally important to ensure the success rate of a ‘mission’, as in my case; a completed thesis. Therefore, there are a list of people that I personally owe a ‘thank you’ note.

First and foremost, I would like to express my appreciation to my supervisor, Assoc. Prof. Dr. Saw Kim Guan and for his never ending patience, support, guidance, advice, time and encouragement throughout my candidature period. I am also would like to thank my co-supervisor, Dr. Yam Fong Kwong for his help and support whenever in need.

The thesis would not be completed without the help and guide especially on the technical aspects. So, my thank goes to the technical help and support from the INOR Lab personnel; Ms. Ee Bee Choo, Mr. Hazhar, Mr. Anas, Mr. Abdul Jamil and Mr. Yushamdan, the Electron Microscope Unit personnel; Ms. Jamilah, as well as fellow seniors and peer students.

Last but not least, my gratitude goes towards my supportive and beloved husband, my kids, my parents and family. Thank you for the all the love, strength and motivation that always give me a reason to accomplish my mission.

## TABLE OF CONTENTS

Acknowledgement	ii
Table of contents	iii
List of Tables	vii
List of Figures	viii
List of Abbreviations	xii
List of Symbols	xiv
Abstrak	xv
Abstract	xviii

## **CHAPTER 1 – INTRODUCTION**

1.1 The growth of ZnO	2
1.2 The suitability of ZnO for TCO applications	4
1.3 Metal doping of ZnO	4
1.4 Motivation	7
1.5 Problem statement	8
1.6 Research objectives	9
1.7 Outline of thesis	9

## **CHAPTER 2 – LITERATURE REVIEW**

2.1	Current research in transparent conductive oxide (TCO) and their applications	10
2.2	Review of the different deposition techniques of IZO thin films	11
2.3	Characterization and properties of metal doped ZnO thin films by sputtering deposition	16
2.3.1	The effect of substrate temperature	17
2.3.2	The effect of dopant content	21
2.3.3	The effect of post-annealing	26

## **CHAPTER 3 – METHODOLOGY**

3.1	Introduction	28
3.2	Sample preparation	28
3.3	Deposition of In-doped ZnO thin films	29
3.4	Characterization of In-doped ZnO thin films	31
3.4.1	Structural properties of In-doped ZnO thin films	34
3.4.1(a)	Scanning electron microscope (SEM)	34
3.4.1(b)	X-ray diffraction (XRD)	35
3.4.1(c)	Raman spectroscopy	37
3.4.2	Optical properties of In-doped ZnO thin films	39
3.4.2(a)	Ultraviolet-visible spectroscopy (UV-VIS)	39
3.4.3	Electrical properties of In-doped ZnO thin films	40
3.4.3(a)	Hall effect system	40

3.5	Annealing	43
-----	-----------	----

3.6	Film thickness measurement	44
-----	----------------------------	----

## **CHAPTER 4 – RESULTS AND DISCUSSION**

4.1	Structural characteristics of In-doped ZnO thin films with various In content	47
-----	---	----

4.1.1	Energy dispersive x-ray spectroscopy (EDX)	47
-------	--	----

4.1.2	X-ray diffraction (XRD)	51
-------	-------------------------	----

4.1.3	Raman spectroscopy	57
-------	--------------------	----

4.1.4	Scanning electron microscopy (SEM) morphology	59
-------	---	----

4.2	Optical properties of In-doped ZnO thin films with various In content	61
-----	---	----

4.3	Electrical properties of In-doped ZnO thin films with various In content	66
-----	--	----

4.4	Substrate temperature effect and film growth properties	69
-----	---	----

4.5	Effect of annealing temperature	74
-----	---------------------------------	----

4.6	Discussion and comparison of structural, optical and electrical properties of In-doped ZnO, Al-doped ZnO & Ga-doped ZnO thin films	79
-----	--	----

## **CHAPTER 5 – CONCLUSION AND FUTURE RECOMMENDATION**

5.1	Conclusion	84
-----	------------	----

5.2	Future work proposal	86
-----	----------------------	----



## LIST OF TABLES

	<b>Page</b>
Table 1.1 Properties of ZnO films with different dopants and fabrication techniques reported in previous studies.	6
Table 2.1 Additional modes wave number observed for the Fe, Al, Sb, and Ga doped ZnO thin film. (Adapted from Bundesmann <i>et al.</i> , 2003)	15
Table 2.2 Summary of the effect of substrate temperature on structural properties of ZnO based thin films by various references.	18
Table 2.3 The average transparency in the visible wavelength of the ZnO thin films doped with various element by references.	23
Table 2.4 Summary of electrical resistivity changes according to dopant content.	24
Table 3.1 Deposition parameters of ZnO and IZO thin films sputtered using RF magnetron sputtering	30
Table 3.2 The thickness data of the un-doped and Indium doped ZnO thin films using Filmetrics measurement.	46
Table 4.1. Weight percentage (wt. %) of Zn, In and O elements in the thin films.	47
Table 4.2. Details of structural parameters obtained from XRD for un-doped ZnO and IZO thin films	52
Table 4.3. E2 Raman peaks of un-doped ZnO and IZO thin films observed at various In content in term of E2/Si ratio. The Raman peak intensity for Si is 1316 a.u.	58
Table 4.4. The extinction coefficient value of the ZnO and IZO thin films at 400 nm.	66
Table 4.5. Weight percentage (wt. %) of Zn, In and O elements in the thin films with various substrate temperature.	70
Table 4.6. Details of structural parameters obtained from XRD for different substrate temperature.	72
Table 4.7. The extinction coefficient value of the ZnO and IZO thin films annealed with different temperature at $\lambda = 400$ nm.	76

## LIST OF FIGURES

	<b>Page</b>
Figure 1.1 ZnO structure representation; (a) cubic rock salt, (b) cubic zinc blend, (c) hexagonal wurtzite. Zn and O atoms represented by shaded gray and black spheres, respectively. (Source: Morkoç and Özgur, 2009)	1
Figure 1.2 Example of Al <sup>+3</sup> dopants substitute Zn <sup>2+</sup> positions in the zinc oxide lattice. (Source: Rhee, 2011)	7
Figure 2.1 SEM images of ZnO and IZO thin deposited with various In content of (a) 0, (b) 1, (c) 2, (d) 3, (e) 4 and (f) 5 at. %. (Source: Kim <i>et al.</i> , 2011)	12
Figure 2.2 The variation of resistivity, mobility and carrier concentration of ZnO and IZO thin films as a function of In concentration. (Source: Chen <i>et al.</i> , 2009)	13
Figure 2.3 XRD spectra of IZO thin films ( $x = 0.90$ ) deposited at different temperatures. (Source: Kim <i>et al.</i> , 2008)	14
Figure 2.4 SEM images of IZO thin films as a function of In content at substrate temperature of 400°C (a) $x = 0.95$ , (b) $x = 0.90$ , (c) $x = 0.80$ . (Source: Kim <i>et al.</i> , 2008)	14
Figure 2.5 The resistivity, carrier concentration and mobility of IZO thin films dependence on Zn content. (Source: Kim <i>et al.</i> , 2008)	16
Figure 2.6 Raman spectra of ZnO thin films with various substrate temperature. (Source: Singh <i>et al.</i> , 2007)	19
Figure 2.7 Raman spectra of AZO thin films sputtered at different substrate temperatures. (Source: Charpentier <i>et al.</i> , 2012)	20
Figure 2.8 XRD spectra of the ZnO and IZO thin film in the range of 1 to 4 wt. % In. Q0 refers to un-doped ZnO, Q1 = 1 wt. % In, Q2 = 2 wt. % In, Q3 = 3 wt. % In, and Q4 = 4 wt. % In. (Source: Binh <i>et al.</i> , 2011)	22
Figure 2.9 XRD spectra of GZO thin film with different Ga <sub>2</sub> O <sub>3</sub> wt. %. (Source: Lee <i>et al.</i> , 2008)	22
Figure 2.10 SEM micrographs of (a) un-doped ZnO, (b) 1 at. % IZO, (c) 3 at. % IZO, (d) 5 at. % IZO, (e) 7 at. % IZO, (f) 9 at. % IZO. (Source: Xie <i>et al.</i> , 2012)	25

Figure 3.1	Flow chart of the substrate cleaning.	29
Figure 3.2	HHV Auto 500 Vacuum Coater with Turbomolecular Pumping System (Nano Optoelectronics Research Laboratory, School of Physics, USM).	31
Figure 3.3	Principle of generation of characteristics radiation. (Source: A manual for JRF/X-ray fluorescence, 2010)	32
Figure 3.4	Signals generated in the interaction volume. (Source: Dehm, 2012)	33
Figure 3.5	Flow chart of the characterization process of IZO thin film.	34
Figure 3.6	Scanning electron microscope, JSM 6460 LV (Nano Optoelectronics Research Laboratory, School of Physics, USM).	35
Figure 3.7	X-ray diffraction schematic arrangement for thin films. (Source: Waseda et al., 2011)	37
Figure 3.8	Simplified diagram of how a Raman spectrometer works.	38
Figure 3.9	Raman Spectroscopy, Jobin Yvon 800 HR UV (Nano Optoelectronics Research Laboratory, School of Physics, USM).	39
Figure 3.10	Schematic diagram of the components of a typical double beam spectrophotometer. (Source: UV-vis spectroscopy, 1987)	40
Figure 3.11	Edwards Auto 306 Coater (Nano Optoelectronics Research Laboratory, School of Physics, USM).	41
Figure 3.12	Hall effects measurement setup.	41
Figure 3.13	HL 5500 PC Hall Effect Measuring System (Nano Optoelectronics Research Laboratory, School of Physics, USM).	43
Figure 3.14	Nabertherm B 150 Tube Furnace (Physics Laboratory, School of Distance Education).	44
Figure 3.15	The reflection of light when it crosses the interface of two different materials. (Source: Filmetrics, Inc., 2012)	45
Figure 4.1	EDX spectra of the ZnO and IZO thin films.	48

Figure 4.2	Correlation between carrier concentration, $n_c$ and In doping content in film (wt. %). The carrier concentration for un-doped ZnO is $2.56 \times 10^{18} \text{ cm}^{-3}$ . The doping of In into Zn increases the carrier concentration.	49
Figure 4.3	In content (wt. %) in film vs. In content (wt. %) in target composition.	50
Figure 4.4	XRD pattern of ZnO and IZO thin films as a function of In content. The inset show the XRD spectra of Z1 sample with wider $2\theta$ range ( $30^\circ \leq 2\theta \leq 80^\circ$ ).	51
Figure 4.5	Graph of lattice constant $c$ of un-doped ZnO and IZO thin films as a function of In content.	53
Figure 4.6	The changes of the lattice constant $c$ against the In content.	54
Figure 4.7	Residual stress of un-doped ZnO and IZO thin films with various In content.	55
Figure 4.8	Raman spectra of un-doped ZnO and IZO thin films with various In wt. %; (a) Si substrate, (b) Z1 (un-doped ZnO), (c) Z2, (d) Z3, (e) Z4 & (f) Z5.	57
Figure 4.9	Surface SEM images of the IZO films with different carrier concentration (100 000 magnifications); <b>a.</b> Z1 (un-doped ZnO), <b>b.</b> Z2, <b>c.</b> Z3, <b>d.</b> Z4 & <b>e.</b> Z5.	60
Figure 4.10	Optical transmittance spectra of un-doped ZnO and In doped ZnO with bare glass spectra as a comparison.	61
Figure 4.11	Variation of $(ahv)^2$ of un-doped ZnO and IZO as a function of photon wavelength.	63
Figure 4.12	Plot of band gap energy vs. wt. % In content.	63
Figure 4.13	Band gap energy shift as a function of carrier concentration.	64
Figure 4.14	The extinction coefficient variation of ZnO and IZO thin film over the wavelength.	65
Figure 4.15	Resistivity, mobility and carrier concentration of un-doped ZnO and IZO thin films as a function of In content.	67
Figure 4.16	Comparison between crystallite size and mean free path length of un-doped ZnO and IZO thin films as a function of In content.	69

Figure 4.17	EDX spectrum of IZO thin film deposited at RT and 150 °C.	70
Figure 4.18	XRD spectra of IZO thin film deposited at 150 °C and RT.	71
Figure 4.19	SEM images of IZO thin film fabricated at RT with different magnification of (a) 10,000x, and (b) 50,000x. The SEM image at 10,000x magnification show the formation of void on the thin film surface, while the SEM image at 50,000x show the poor crystal growth of the IZO thin film.	73
Figure 4.20	SEM image of IZO thin film deposited at substrate temperature of 150 °C at 50,000x magnification.	74
Figure 4.21	Optical transmittance of IZO thin film as a function of annealing temperature.	75
Figure 4.22	Plots of $(\alpha h\nu)^2$ vs. photon energy of IZO thin films with various annealing temperature.	76
Figure 4.23	Extinction coefficient of the IZO thin film with various annealing temperature.	77
Figure 4.24	Variation of electrical properties of IZO thin film as a function of annealing temperature.	78
Figure 4.25	XRD spectra of (a) AZO and (b) GZO thin films as a function of dopant content. (Source: Lu <i>et al.</i> , 2006); Lee <i>et al.</i> , 2008)	80
Figure 4.26	Optical transmittance spectra of (a) AZO and (b) GZO with addition of dopant content. (Source: Lu <i>et al.</i> , 2006); Lee <i>et al.</i> , 2008)	81
Figure 4.27	Plots of $(\alpha h\nu)^2$ vs. photon energy of (a) AZO and (b) GZO thin films with various doping content. (Source: Lu <i>et al.</i> , 2006); Lee <i>et al.</i> , 2008)	82
Figure 4.28	Plots of resistivity, carrier concentration and Hall mobility of GZO thin films as a function of dopant content. (Source; Lee <i>et al.</i> , 2008)	82

## **LIST OF ABBREVIATIONS**

AAO	Anodic Aluminium Oxide
Al	Aluminium
AZO	Aluminium Zinc Oxide
CCD	Charged couple device
CVD	Chemical vapour deposition
DC	Direct current
DMSO	Dimethyl Sulphoxide
EDX	Energy dispersive x-ray
F	Fluorine
Fe	Iron/Ferum
FWHM	Full width half maximum
Ga	Gallium
Ga <sub>2</sub> O <sub>3</sub>	Gallium Oxide
GaN	Gallium Nitride
GZO	Gallium Zinc Oxide
In	Indium
In <sub>2</sub> O <sub>3</sub>	Indium Oxide
ITO	Indium Tin Oxide
IZO	Indium Zinc Oxide
K	Potassium/Kalium
KOH	Potassium/Kalium Hydroxide
LF	Low frequency
Li	Lithium
LiOH	Lithium Hydroxide
LO	Longitudinal optical
MBE	Molecular beam epitaxy
N	Nitrogen
N <sub>2</sub> O	Nitrous Oxide
NIR	Near infra-red
O <sub>2</sub>	Oxygen

PES	Polyether Sulfone
PET	Polyethylene Terephthalate
PI	Polyimide
PLD	Pulsed laser deposition
RF	Radio frequency
Sb	Antimony
sccm	Standard cubic centimetre
SEM	Scanning electron microscope
TCO	Transparent conducting oxide
TFT	Thin film transistor
TO	Transverse optical
UV	Ultra violet
UV-vis	Ultraviolet - visible
wt. %	Weight percentage
XRD	X-ray diffraction
Zn	Zinc
ZnO	Zinc Oxide
ZnS	Zinc Sulfide

## LIST OF SYMBOLS

$a$	lattice parameter in ‘a’ plane
$c$	lattice parameter in ‘c’ plane
$E_g$	band gap energy
$G$	average crystallite size
$h$	Planks constant
$hv$	photon energy
$k$	extinction coefficient
$l_e$	mean free path
$n_c$	carrier concentration
$q$	fundamental unit of electric charge
$T$	transmittance
$\alpha$	absorption coefficient
$\beta$	full width at half maximum
$\theta$	Bragg diffraction angle
$\lambda$	wavelength
$\mu$	mobility, and
$\rho$	resistivity
$\sigma$	stress

**KESAN PENDOPAN INDIUM KE ATAS CIRI-CIRI STRUKTUR, OPTIK  
DAN ELEKTRIK FILEM NIPIS ZINK OKSIDA**

**ABSTRAK**

Konduktif oksida lutsinar (TCO) seperti filem nipis zink oksida ( $ZnO$ ) didopkan logam mempunyai aplikasi penting dalam peranti optoelektronik. Filem nipis  $ZnO$  didopkan logam mempunyai kelebihan kerana mereka boleh difabrikasikan dalam proses yang agak mudah dan menjimatkan. Walau bagaimanapun, ciri-ciri tersebut adalah sensitif kepada jumlah logam pendopan di dalam hos bahan zink oksida. Dalam kajian ini, kesan kandungan indium (In) dan juga suhu penyepuhlindapan pada sifat-sifat struktur, optik dan elektrik  $ZnO$  disiasat. Melalui percikan magnet frekuensi radio (RF) dari target  $ZnO$  /  $In_2O_3$  tersinter dengan kandungan In berbeza di antara 1-7 wt. %, filem nipis indium zink oksida (IZO) telah berjaya ditumbuhkan ke atas substrat Si (100) dan substrat kaca yang telah dibersihkan secara ultrasonik. Filem nipis IZO telah ditumbuhkan dalam persekitaran argon pada suhu  $150^{\circ}C$  dengan kuasa 100W. Selain daripada unsur-unsur zink (Zn) dan oksigen (O), spektrum tenaga serakan sinar-X (EDX) juga mengesan unsur In daripada filem nipis IZO, menunjukkan bahawa In telah berjaya diserapkan ke dalam hos bahan ( $ZnO$ ). Mikroskop imbasan elektron (SEM) menunjukkan bahawa filem-filem nipis IZO mempunyai morfologi permukaan yang berterusan tanpa kehadiran zarah-zarah asing. Filem nipis  $ZnO$  tanpa dop juga difabrikasikan melalui kondisi percikan yang sama untuk perbandingan. Analisis pembelauan sinar-X (XRD) menunjukkan bahawa filem nipis mempunyai kecenderungan orientasi di sepanjang satah (002). Dengan pertambahan kandungan In, kedudukan puncak (002) filem nipis IZO telah beranjak

ke sudut lebih rendah berbanding sampel ZnO tanpa dop. Di samping itu, apabila kandungan In bertambah, saiz hablur menjadi lebih kecil manakala pemalar kekisi  $c$  memanjang kerana lebih banyak In memasuki kekisi ZnO. Spektra Raman mempamerkan mod  $E_2$  (tinggi) pada kedudukan  $437\text{ cm}^{-1}$  seperti jangkaan sepadan dengan struktur wurzit heksagonal ZnO. Walau bagaimanapun, semakin kandungan In bertambah, keamatian mod  $E_2$  (tinggi) berkurangan, menandakan struktur wurzit heksagonal mengalami sedikit kemerosotan. Kemerosotan struktur wurzit heksagonal diperhatikan melalui analisis Raman lantas memberi bukti sokongan terhadap perubahan struktur daripada data XRD. Penambahan kandungan In juga memperkenalkan puncak ganjil di kedudukan  $274\text{ cm}^{-1}$  yang berkaitan dengan kecacatan intrinsik kekisi tuan rumah. Walaupun kajian-kajian yang terdahulu mengaitkan puncak ganjil di kedudukan  $274\text{ cm}^{-1}$  disebabkan oleh mod getaran lokal nitrogen (N), namun kemudiannya ditunjukkan bahawa filem nipis ZnO didopkan dengan logam bendasing yang lain, tanpa kehadiran N juga menghasilkan mod puncak ganjil yang sama. Pemindahan optik mencapai  $\sim 75 - 90\%$  ketelusan dalam rantau penglihatan. Jurang jalur optik (jurang Tauc) ZnO tanpa dop melebar daripada  $3.29\text{ eV}$  kepada  $3.48\text{ eV}$  di permulaan pendopan In diikuti dengan penyempitan jurang jalur bagi pertambahan lebih banyak kandungan In. Pelebaran jurang jalur dapat dijelaskan dengan anjakan Burstein Moss, di mana kemasukan kandungan logam dopan yang mencukupi menganjak pinggir penyerapan ke tenaga yang lebih tinggi, dengan itu, melebarkan jurang jalur optik. Dengan dopan In yang lebih tinggi, jurang jalur menyempit daripada  $3.48\text{ eV}$  kepada  $3.28\text{ eV}$  akibat dari pembentukan hujung keadaan di bawah pinggir jalur konduksi. Ion-ion  $Zn^{2+}$  di tapak kekisi Zn digantikan oleh ion-ion  $In^{3+}$ , proses tersebut menyebabkan ketumpatan pembawa menjadi lebih tinggi. Ketumpatan pembawa filem nipis IZO meningkat daripada  $10^{18}$  kepada  $10^{20}$

$\text{cm}^{-3}$  dengan peningkatan kandungan In. Di samping itu, bukti tidak langsung penggantian Zn oleh In diperoleh daripada hubungan yang hampir linear di antara kandungan In dan perubahan pemalar kekisi  $c$  filem nipis IZO yang selaras dengan hukum Vegard. Kerintangan ZnO tanpa dop adalah  $3.037 \Omega \text{ cm}$  manakala nilai kerintangan paling rendah bagi sampel IZO adalah  $3.09 \times 10^{-3} \Omega \text{ cm}$ . Untuk sampel IZO yang disepuh lindap di udara dalam julat suhu di antara  $300 - 500^\circ\text{C}$  selama 40 min, pemindahan optik kekal pada  $\sim 75 - 90\%$  di rantaui penglihatan manakala jurang jalur optik mengecil daripada  $3.42\text{eV}$  (tanpa sepuh lindap) kepada  $3.21\text{eV}$ . Penyepuh lindapan pada suhu  $500^\circ\text{C}$  menyebabkan kerintangan meningkat kepada  $1.972 \times 10^2 \Omega \text{ cm}$ , menjadikannya kurang konduktif daripada sampel yang tidak disepuh lindap ( $1.285 \times 10^{-2} \Omega \text{ cm}$ ).

# **EFFECT OF INDIUM DOPING ON STRUCTURAL OPTICAL AND ELECTRICAL PROPERTIES OF ZINC OXIDE THIN FILMS**

## **ABSTRACT**

Transparent conducting oxide (TCO) such as metal-doped zinc oxide ( $ZnO$ ) thin films have important applications in optoelectronic devices. Metal-doped  $ZnO$  thin films have an advantage as they can be fabricated in a relatively simple and economical process. However, their properties are sensitive to the amount of metal doping in the zinc oxide host material. In this work, the effect of indium (In) content as well as the annealing temperature on the structural, optical and electrical properties of  $ZnO$  were investigated. The Indium-doped  $ZnO$  (IZO) thin films were successfully deposited onto ultrasonically cleaned Si (100) and glass substrates by radio frequency (RF) magnetron sputtering from sintered  $ZnO/In_2O_3$  target with different In content ranging from 1 to 7 wt. %. The IZO thin films were grown in argon environment at 150°C with a bias power of 100W. Apart from zinc (Zn) and oxygen (O) elements, the energy dispersive x-ray (EDX) spectra of the IZO thin films also detected In element, indicating that In were successfully incorporated into the host material ( $ZnO$ ). The scanning electron microscopy (SEM) shows that the IZO thin films have a continuous surface morphology without the presence of foreign particles. Un-doped  $ZnO$  films were also fabricated under the same sputtering conditions for comparison. The X-ray diffraction (XRD) analysis show that the thin films have preferential orientation along (002) plane. With increasing In content, the (002) peak position of the IZO thin films were shifted to lower angles when referenced to the un-doped  $ZnO$  sample. In addition, as the In content increases, the crystallite size becomes smaller while the lattice

constant  $c$  elongates due to the incorporation of more In into ZnO lattice. The Raman spectra reveals the expected  $E_2$  (high) mode at  $437\text{ cm}^{-1}$  corresponding to the ZnO hexagonal wurtzite structure. However, as the In content increases, the intensity of  $E_2$  (high) mode reduces indicating a slight deterioration of hexagonal wurtzite structure. The deterioration of the hexagonal wurtzite structure observed by the Raman analysis thus provides corroborating evidence of structural changes from the XRD data. The addition of In also introduces anomalous peak at  $274\text{ cm}^{-1}$  related to intrinsic host lattice defect. Although previous studies relates the anomalous peak at  $274\text{ cm}^{-1}$  to the nitrogen (N) induced local vibration mode, it was later shown that the ZnO thin film doped with other metal impurities, without the presence of N also produces the same anomalous mode. The optical transmittance reaches  $\sim 75 - 90\%$  transparency in the visible region. The optical band gap (Tauc gap) widens from  $3.29\text{ eV}$  for the un-doped ZnO to  $3.48\text{ eV}$  with initial In doping followed by band gap narrowing with further addition of In content. The band gap widening can be explained by the Burstein Moss shift where the incorporation of sufficient metal dopant content shifts the absorption edge to higher energies, thus, widening the optical band gap. With higher In doping, the band gap narrows from  $3.48\text{ eV}$  to  $3.28\text{ eV}$  as a result of band tail states formation below the conduction band edge. The  $Zn^{2+}$  ions at Zn lattice sites are substituted by the  $In^{3+}$  ions, resulting in higher carrier concentration in the process. The carrier concentration of the IZO thin films increases from  $10^{18}$  to  $10^{20}\text{ cm}^{-3}$  with increasing In content. In addition, indirect evidence of substitution of Zn by In is obtained from a nearly linear relationship between the In content and the changes of the lattice constant  $c$  of the IZO thin films which is in accordance to Vegard's Law. The resistivity of the un-doped ZnO is  $3.037\text{ }\Omega\text{ cm}$  while the lowest resistivity value of the IZO sample is  $3.09 \times 10^{-3}\text{ }\Omega\text{ cm}$ . For IZO samples annealed in air within the range of  $300 - 500^\circ\text{C}$  for

40 min, the optical transmittance is maintained at  $\sim 75 - 90\%$  in the visible region while the optical band gap narrows from 3.42eV (un-annealed) to 3.21eV. Annealed at 500°C caused the resistivity to increase to  $1.972 \times 10^2 \Omega \text{ cm}$ , making it less conductive than the un-annealed sample ( $1.285 \times 10^{-2} \Omega \text{ cm}$ ).

# CHAPTER 1

## INTRODUCTION

ZnO has attracted keen research interest in recent years due to its promising properties for opto-electronics, biomedical and many other applications. It occurs naturally as zincite. Unfortunately, this mineral form of ZnO is rare in nature and thus cannot be used on a commercial scale. ZnO usually crystallizes in the form of wurtzite (as in the case of zincite) or zinc blende structure. The wurtzite structure is commonly found for ZnO due to the stability in ambient conditions. The zinc blend structure may be stabilized if grown on substrates with cubic structure. ZnO also may crystallize in rock salt phase. The existence of the ZnO with various structures is shown in Figure 1.1.

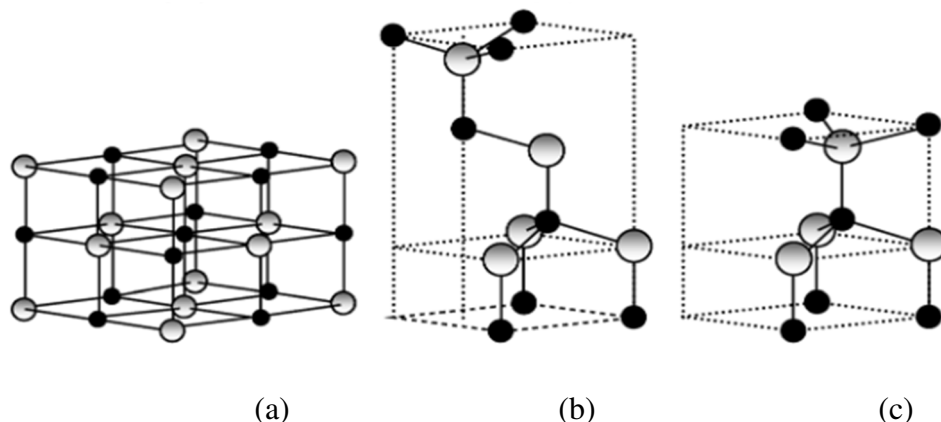


Figure 1.1. ZnO structure representation; (a) cubic rock salt, (b) cubic zinc blend, (c) hexagonal wurtzite. Zn and O atoms represented by shaded gray and black spheres, respectively. (Source: Morkoç & Özgur, 2009)

The wurtzite structure is usually found in ZnO thin films. According to Coleman & Jagadish (2006), the ideal lattice parameter  $a$ , and  $c$ , of the ZnO hexagonal wurtzite structure is  $\sim 0.325$  nm and  $0.512$  nm respectively. However, the structural properties

of the ZnO may change according to the growth conditions such as the applied power, substrate temperature, growth pressure and atmosphere, as well as the dopant content. As an example, Benouis *et al.* (2010) reported the changes of the lattice parameters  $c$  of the un-doped ZnO thin film fabricated from spray pyrolysis technique from 5.213 nm to 5.169 nm for the ZnO thin film doped with 3 at. % In. Their work implies that the addition of a metal dopant or impurity may be used to tailor the properties of ZnO thin film, which is an important material for current opto-electronic devices. The phenomenon of adding a metal dopant into ZnO is used to make transparent conducting oxides (TCO). Here, the incorporation of metal dopants generally reduces the resistivity but the onset of metal-like conductivity in ZnO depends on the type of metal as well as the crucial amount. Metals such as In, Al or Ga are currently attracting keen research interest to achieve better ZnO-based TCOs. At the same time the metal dopant should not decrease the transmittance of ZnO. Since ZnO cannot be mined naturally but is a much sought after material, it is grown using various methods where metal impurities or dopants can be added to change its properties.

## 1.1 The growth of ZnO

ZnO in polycrystalline form is largely used as a facial powders, sunscreens, catalysts and paint pigmentation. In an optoelectronic applications, ZnO in the form of single crystal or thin films is required. The ZnO can be fabricated into several form depending on the growth techniques such as the gas transport, hydrothermal and pressurized melt growth (Janotti & Van de Walle, 2009). For instance, using the gas transport technique, ZnO platelets or hexagonal needles can be produced from zinc vapor in a low temperature region at an ambient environment. Large single ZnO crystals can growth hydrothermally within 300 to 400 °C in a platinum lined autoclave.

At high temperature and pressure, KOH/LiOH base solution is used to dissolve the ZnO. Then, the dissolved ZnO is precipitated at low temperature forming ZnO crystal with diameter up to 2 inches. Hydrothermal method may provide an advantage in term of low temperature growth, but it also offered some weakness. Aside from the slow growth rate, the ZnO crystal growth from hydrothermal method may be contaminated with the solvent derived impurities such as Li and K, indirectly affecting the properties of the ZnO samples. In pressurized melt growth technique, the ZnO placed in a crucible were melted by a heat source. The cooled ZnO layer in a form of single crystal is isolated from the crucible, reducing the risk of contamination due to contact with the crucible.

Many techniques have been explored to grow the ZnO thin films including sol gel (You, 2013; Chen *et al.*, 2010; Rezaee *et al.*, 2009; Singh *et al.*, 2011), thermal evaporation (Palimar *et al.*, 2012), chemical spray pyrolysis (Illican *et al.*, 2006; Illican *et al.*, 2008; Wang, 2004; Singh *et al.*, 2010), pulsed laser deposition (PLD), sputtering, chemical vapor deposition (CVD), and molecular beam epitaxy (MBE). The advantages associated with sol gel technique are the deposition of high purity, homogenous and requires relatively low temperatures. But the technique also requires longer processing time, involving harmful chemical solvents and relatively higher cost of the raw material (Rezaee *et al.*, 2009). Both chemical spray pyrolysis and thermal evaporation provides simple and low cost procedure. For chemical spray pyrolysis technique, the quality issue of the thin films may be a problem. In thermal evaporation technique, the chemical interaction between the charge and the crucible may occurred, thus, disrupting the growth of the thin film. So far, sputtering provides the best solution for thin films fabrication in mass production because of the high deposition rate. It is a popular method used in industry.

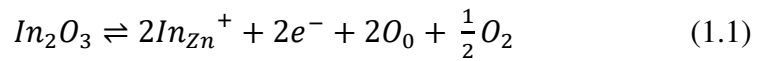
## **1.2 The suitability of ZnO for TCO applications**

The use of ZnO as a semiconductor material has attracted keen research in recent years because of its large area of applications. As a member of the II-IV semiconductor group which possess a wide band gap of ~3.3 eV at room temperature, ZnO is a potential material for optoelectronic devices (Jie *et al.*, 2004). Due to the wide band gap, ZnO ability to remain transparent in the visible wavelength region has present a major driving force of research as its prospective use in thin film solar cells (Guillén & Herrero, 2010; Binh *et al.*, 2011), flat panel display (Jie *et al.*, 2003), gas sensors, and light emitting devices in the visible and ultraviolet (UV) region (Rambu *et al.*, 2012). The wide band gap also provided advantages such as allowing the ZnO based devices to operate at high voltages and higher temperature. ZnO has a huge exciton binding energy ~60 meV, which is twice larger than gallium nitride, GaN (~28 meV). The large exciton binding energy makes the exciton well separated from conduction band at room temperature ( $kT_{room} = 25$  meV). Moreover the higher binding energy enhances the efficiency of light emissions, giving advantage over GaN for exciton-related device applications (Kim *et al.*, 2000).

## **1.3 Metal doping of ZnO**

Controlling the conductivity of ZnO thin films has always been a major consideration. As deposited ZnO exhibits n-type conductivity in nature. The source of free electrons contributing to the n-type conductivity in ZnO has been widely debated and remain inconclusive. One of the most popular explanations suggests that native point defects such as vacancies and interstitials within the ZnO host lattice causes the n-type conductivity in the as-grown ZnO (Laks *et al.*, 1992). The difficulties to achieve the p-type ZnO through doping is believed due to the self-compensation effect of ZnO

by native point defects (Pearton *et al.*, 2005). Doping is an intentional process of introducing impurities into a semiconductor for the purpose of modulating its optoelectrical properties. The changes in conductivity by orders of magnitude with the introduction of metal oxides of different valencies to ZnO have been reported. When the group III oxides such as In<sub>2</sub>O<sub>3</sub> is added to ZnO, it is believed that the In occupies the Zn lattice sites contributing two electrons for the bonding. The extra electron is freed to the conduction band according to the equation (Ellmer *et al.*, 2008);



The increasing free electrons thus reduces the electrical resistivity. The electrical resistivity for ZnO varies from 10<sup>-1</sup> to 10<sup>-4</sup> Ω cm with carrier concentration of ~10<sup>16</sup> cm<sup>-3</sup> at room temperature (Jagdish & Pearton, 2006). Palimar *et al.* (2012) reported that the room temperature resistivity of 1.72 x 10<sup>-3</sup> Ω cm is obtained when ZnO is doped with indium (In). Czternastek *et al.* (2004) reported that doping up to 3% Aluminum (Al) showed resistivity of 1.3 x 10<sup>-3</sup> Ω cm on the doped ZnO thin films. High optical transmittance within the visible region is achievable for doped ZnO thin film depending on the percentages of the metallic dopant. Indium doped ZnO (IZO) thin films fabricated through spray pyrolysis technique shows high optical transmittance percentage of 80% to 90% (Benouis *et al.*, 2010; Singh *et al.*, 2010). In previous study by Kim *et al.* (2012), Al doped ZnO (AZO) thin films fabricated from sol gel spin on quartz substrate exhibit a high optical transparency of about 80% in the visible range. However, higher percentages of dopants will drastically reduce the optical transmittance. It is therefore important to explore the effects of the dopant amount and its dependence on the optical transmittance. Table 1.1 shows the ZnO thin films doped

with various dopant by different deposition technique and its opto-electrical properties. The changes of the electrical and the optical properties of ZnO thin film are observed when the amounts and the types of the dopant changed. With doping, ZnO which is semiconducting in nature will change into metallic like conductivity. A semiconductor-to-metal transition occurs in degenerate semiconductors such as ZnO at sufficiently high doping concentration.

Table 1.1. Properties of ZnO films with different dopants and fabrication techniques reported in previous studies.

Dopant	Optimum content in target (wt. %)	Magnitude of Resistivity ( $\Omega \text{ cm}$ )	T (%)	Technique	References
<b>Al</b>	2	$10^{-3}$	>85%	Sputtering	Guillén & Herrero, 2010
<b>Ga</b>	5	$10^{-4}$	85%	Sputtering	Kim <i>et al.</i> , 2009
<b>In</b>	10	$10^{-4}$	>90%	Sputtering	Shin <i>et al.</i> , 2009
<b>F</b>	2	$10^{-4}$	>90%	PLD	Liu <i>et al.</i> , 2013
<b>Si</b>	2	$10^{-4}$	~80%	PLD	Liu <i>et al.</i> , 2013

These dopants ( $\text{In}^{3+}$ ,  $\text{Al}^{3+}$ , or  $\text{Ga}^{3+}$ ) act as a donor when it substitute the position of  $\text{Zn}^{2+}$  at the ZnO lattice sites (Rambu *et al.*, 2012). Figure 1.2 show the example of metal dopant substituting the  $\text{ZnO}^{2+}$  position in the ZnO lattice sites.

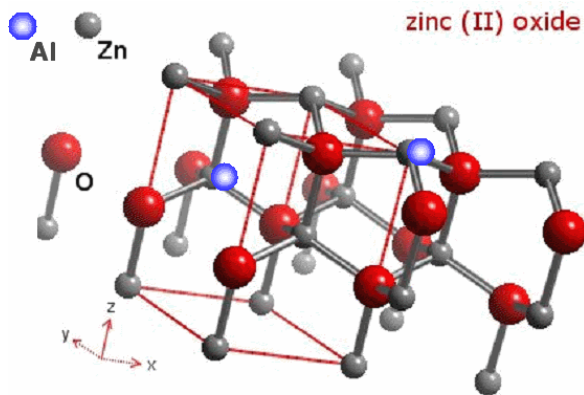


Figure 1.2. Example of  $\text{Al}^{+3}$  dopants substitute  $\text{Zn}^{2+}$  positions in the zinc oxide lattice. (Source: Rhee, 2011)

#### 1.4 Motivation

One of the highly potential  $\text{ZnO}$  based material is the Indium doped  $\text{ZnO}$  or known as IZO. Previous work on the IZO thin film fabricated through various deposition technique has been widely reported. However, the IZO thin film deposited by the sputtering method is not well reported in literature. Most of the IZO thin film was sputtered at elevated temperature. For example, in the work of Kim & Park (2001), the substrate temperature was kept at  $500\text{ }^{\circ}\text{C}$  during deposition of the IZO thin film. In the present work, a lower substrate temperature for the deposition of IZO thin film by sputtering will be attempted as it is more economical. The electrical and optical properties of the samples deposited at a lower substrate temperature in this study will be investigated and discussed.

Transparent conductive oxides (TCOs), with the ability to appear transparent in the visible light and the capabilities of transporting electrical charge are important in optoelectronic devices.  $\text{ZnO}$  is included as one of the most common TCOs nowadays. The IZO thin film has attracted keen interest as a promising alternative material for the currently used indium tin oxide or ITO. However, the high demand of the ITO in the market has faced difficulties due to unstable supply of the ITO, which also expensive.

The choice of the IZO thin film in turn uses ZnO which can be produced abundantly and economically. This ZnO based TCO is also relatively inexpensive and nontoxic (Liu *et al.*, 2013).

### **1.5 Problem statement**

IZO possess high potential in semiconductor device applications especially as a TCO material which has metal-like conducting properties while remaining transparent within the visible region of the wavelength. These properties makes good transparent electrodes for flat panel displays, solar cells and organic light emitting diodes (LEDs). As with all thin film applications, the successful use of IZO as a TCO depends on two important factors. Firstly, quality growth of the thin films on substrates must be realized. This requires that an uncontaminated and continuous film can be deposited without any regions of voids or cracks. It also implies that the film does not delaminate due to film stress. The first condition requires a suitable fabrication technique that does not inadvertently introduce contaminations into the thin film and also implies that the deposition parameters such as substrate temperature that affect nucleation and growth must be set right.

Secondly the dependence of the properties of the IZO films on the amount of In dopants must be investigated. An amount that is less may not produce metal-like conductivity while a large amount is likely to cause undesired structural, electrical and optical properties. Adding even small amounts of In can introduce various types of defects into the ZnO host lattice.

Therefore, understanding the effects of doping with metal impurities and preparation conditions on the optical, electrical and structural properties of ZnO is the key towards successful application in optoelectronic devices.

## **1.6 Research objectives**

The objectives of the research are to investigate;

- i. the effect of various wt. % of In doping on the structural properties such as lattice constant, crystallite size and the film stress;
- ii. the effect of various wt. % of In doping on electrical such as resistivity, carrier concentration and mobility;
- iii. the effect of various wt. % of In doping on the optical properties such as transmittance, optical band gap and extinction coefficient;
- iv. the effect of annealing on the electrical and optical properties of IZO thin films

## **1.7 Outline of the thesis**

Chapter 2 gives the literature review on the findings of previous studies of ZnO with metal doping, current issues and motivation on the development of ZnO and its application. Some discussion of using sputtering technique to fabricate the ZnO thin films also discussed.

Chapter 3 describes the process of sample preparation and fabrication. The description of the procedures involved as well as the characterization techniques used to investigate the electrical, optical and structural properties of the samples such as X-ray diffraction (XRD), scanning electron microscopy (SEM), energy dispersive spectroscopy (EDX), Raman spectroscopy, UV-Visible (UV-VIS) spectrophotometry and Hall effect is presented.

Chapter 4 presents the results obtained in this work and the related discussion.

Chapter 5 summarizes the conclusions drawn from this research and gives suggestions for future work.

## CHAPTER 2

### LITERATURE REVIEW

#### **2.1 Current research in transparent conductive oxide (TCO) and their applications**

The transparent conductive oxides (TCOs) can be regarded as a material that possess a metal-like conducting properties while remain transparent within the visible region of the wavelength. One of the most popular TCO is ZnO as well as ZnO based materials. Research on ZnO based material has been done extensively as it offered a promising alternative material for the expensive ITO thin films in transparent electrode application. ZnO also holds potential in device application due to near similarities in the structural and optical properties between ZnO and GaN. The high exciton binding energy of ZnO (~60 meV) serves as an advantage in optoelectronic devices such as light emitting and laser diodes (Kim *et al.*, 2001).

A high optical transmittance of 75% in the visible region is attractive for optoelectronic devices applications such as transparent thin film transistor (Hoffman *et al.* 2003). The usage of ZnO as transparent conductive electrode flat panel display has been reported in numerous studies (Ito *et al.*, 2005; Shin *et al.*, 2009). ZnO thin films are commonly fabricated onto various types of substrates. Shin *et al.* (2009) successfully deposited IZO thin film at room temperature using DC magnetron sputtering, having a resistivity of the order of  $10^{-4} \Omega \text{ cm}$  onto polyethylene (PET) substrate. In another report, the IZO thin film fabricated onto polyether-sulfone (PES) substrate was found to exhibit high optical transparency of over 82% with minimum sheet resistance of  $29 \Omega/\text{sq}$ . at optimal condition (Kim *et al.*, 2007).

Currently, there is keen interest in IZO to investigate the effects of In doping on the properties of this ZnO based TCO material. A review of the effect of In doping and the properties of IZO is presented in the following section.

## **2.2 Review of the different deposition techniques of IZO thin films**

Many approaches are explored to fabricate the IZO thin film, including chemical routes and physical vapor deposition technique. The growth of the fabricated thin film may differ according to the choices of the fabrication technique. Therefore, a same material growth by different techniques may result in different physical properties due to the variation of deposition parameters in each of the techniques. The changes in physical properties such as the structure and morphology due to the introduction of impurities may as well changes the optical and electrical properties of the material. Aside from sputtering technique that is used in this work, the sol gel and pulse laser deposition (PLD) are also popular choices for the growth of the IZO thin film.

Kim *et al.* (2011) fabricated the IZO thin films by the sol gel method on quartz substrate. The work was meant to investigate the effect of In content in the range of 0 to 5 at. % on the structural and optical properties of IZO thin film. The structural analyses of the IZO thin films by means of SEM characterization shows that the ZnO and IZO thin film surfaces consist of grains as shown in Figure 2.1. The continuous grain structure is commonly reported in the IZO fabricated by the sol gel method (Chen *et al.*, 2009). The addition of more In does not hinder the formation of continuous surface morphology. From the SEM images, it seems that grains of the IZO samples are not regular.

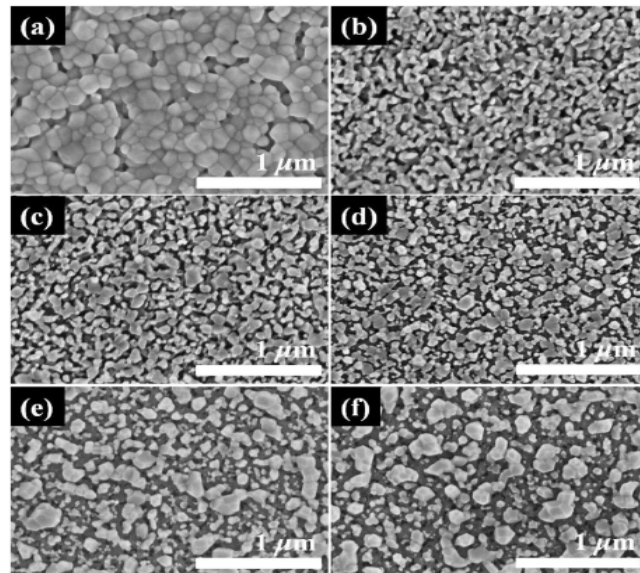


Figure 2.1. SEM images of ZnO and IZO thin deposited with various In content of (a) 0, (b) 1, (c) 2, (d) 3, (e) 4 and (f) 5 at. %. (Source: Kim *et al.*, 2011)

The XRD pattern from Kim *et al.* (2011) reveals that the ZnO and IZO thin films exhibit (002) peak alongside other ZnO peaks indicating hexagonal wurtzite structure. The (002) peak intensity increases to the maximum when doped with 3 at. % In but decreases when doped with more In content (Kim *et al.*, 2011). The crystalline quality improves with the addition of In up to 3 at. %. Similarly, it has been reported that the crystallinity of the IZO thin film is enhanced with adequate amount of In incorporation (Rezaee *et al.*, 2009; Chen *et al.*, 2009). However, further addition of In content decreases the (002) intensity, thus, deteriorates the crystal quality of the IZO thin films.

For optical properties, the addition of In content in the sol gel method seems to reduce the optical band gap of the IZO thin films from 3.2906 to 2.560 eV (Kim *et al.*, 2011). Other papers on sol gel method for the fabrication of the IZO thin film also reported the decrease in band gap value with the addition of dopant content such as the work of Rezaee *et al.* (2009) and Singh *et al.* (2011). The changes on the electrical properties of IZO thin films prepared by the sol gel method with In dopant were

reported in the work of Chen *et al.* (2009). Figure 2.2 shows the electrical properties of un-doped and ZnO thin films doped with 5 and 9 at. % In prepared at 700 °C. The carrier concentration increases with increasing In content up to 9 at. %, from approximately  $10^{14} \text{ cm}^3$  (un-doped sample) to  $10^{21} \text{ cm}^3$ . The resistivity reduces from  $10^3 \Omega \text{ cm}$  for the un-doped sample to the minimum value of  $10^{-1} \Omega \text{ cm}$ . The mobility is reduced as a result of more grain boundary formation (Chen *et al.*, 2009).

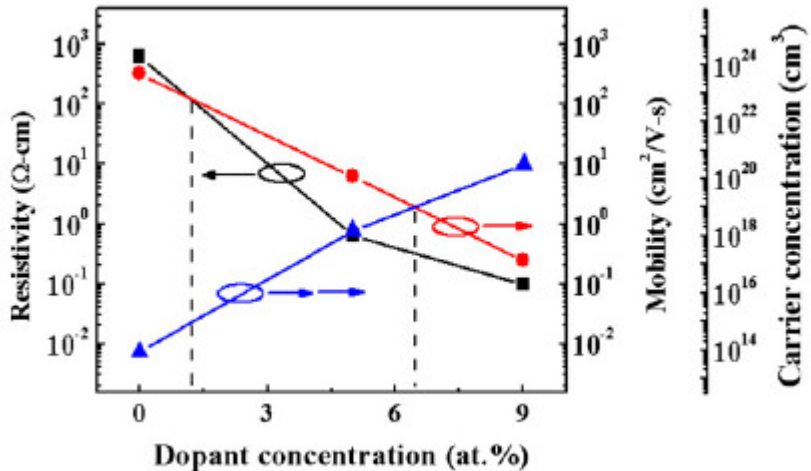


Figure 2.2. The variation of resistivity, mobility and carrier concentration of ZnO and IZO thin films as a function of In concentration. (Source: Chen *et al.*, 2009)

It is interesting to note that IZO thin film with different In percentage fabricated by PLD method exhibited different XRD pattern. In the study of Naghavi *et al.* (2000), the XRD spectra of the IZO thin film with  $\text{In} / (\text{Zn} + \text{In}) = 0.85$  is dominated by (222) orientation. The IZO thin film with lower In content ( $\text{In} / (\text{Zn} + \text{In}) = 0.67$ ) show the presence of (002) reflections of ZnO wurtzite structure. Similarly, Kim *et al.* (2008) also reported the domination of the (222) reflections of IZO thin films with high In content fabricated via PLD at 250 °C. In their work, the IZO thin film is prepared as a function of substrates temperatures within the range of 200 to 550 °C. At 200 °C, no peak is observed in the XRD spectrum as in Figure 2.3, indicating the IZO thin film is

having an amorphous structure (Kim *et al.*, 2008). Interestingly, the IZO thin films deposited by PLD on polyethylene terephthalate (PET) substrates in the work of Socol *et al.*, 2012 also showing amorphous structure.

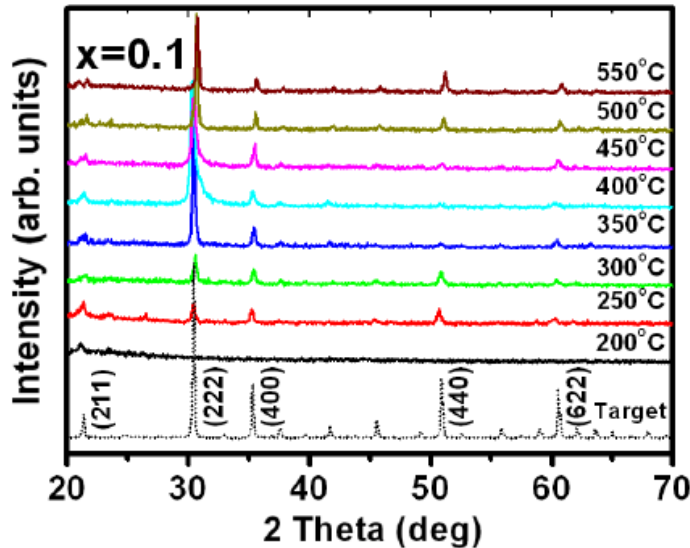


Figure 2.3. XRD spectra of IZO thin films ( $x = 0.90$ ) deposited at different temperatures using PLD. (Source: Kim *et al.*, 2008)

The SEM images of IZO thin film with different Zn content as shown in Figure 2.4 were observed to have continuous, void-free surface.

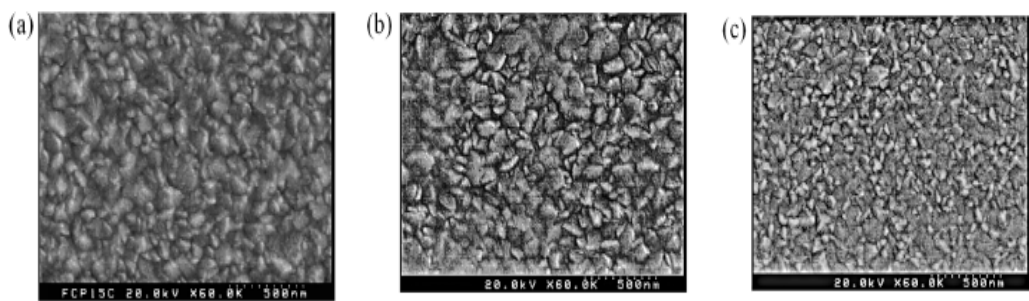


Figure 2.4. SEM images of IZO thin films as a function of In content at substrate temperature of 400°C (a)  $x = 0.95$ , (b)  $x = 0.90$ , (c)  $x = 0.80$ . (Source: Kim *et al.*, 2008)

The dependence of Raman scattering in metal doped ZnO thin films against the dopant elements is demonstrated by Bundesmann *et al.*, 2003. Dopant such as Fe, Sb, Al, and Ga were introduced onto ZnO thin films by PLD technique on sapphire substrate. All of the doped ZnO thin films were grown under pure oxygen ( $O_2$ ) atmosphere except for the other Ga doped ZnO sample that was deposited under nitrous oxide ( $N_2O$ ) atmosphere. Aside from the expected Raman mode that belong to ZnO and sapphire ( $379\text{ cm}^{-1}$ ,  $417\text{ cm}^{-1}$ ,  $430\text{ cm}^{-1}$ ,  $447\text{ cm}^{-1}$ ,  $576\text{ cm}^{-1}$ , and  $749\text{ cm}^{-1}$ ), the Fe, Sb, Al, and Ga doped films reveals additional modes in the Raman spectra as tabulated in Table 2.1.

Table 2.1. Additional modes wave number observed for the Fe, Al, Sb, and Ga doped ZnO thin film. (Adapted from Bundesmann *et al.*, 2003)

Sample	Dopant content (%)	Additional modes ( $\text{cm}^{-1}$ )
ZnO:Fe	8	277, 513, 584, 624, 644, 713, 720
ZnO:Sb	0.5	277, 511, 531, 583, 644, 685
ZnO:Al	2	276, 509, 579, 623, 643
ZnO:Ga	0.5 – 5	277, 631
ZnO:Ga ( $N_2O$ atmosphere)	0.1	277, 512, 583, 624, 644

The earlier perception that the additional modes at  $277$ ,  $513$ ,  $583$  and  $644\text{ cm}^{-1}$  lines is assigned to the incorporation of nitrogen (N) can be denied as the Fe, Sb, Al and Ga doped grown in N free atmosphere also reveals those additional modes. Interestingly, some of the additional modes appeared in the Raman spectra according to the dopant element. For example, the additional mode at  $720\text{ cm}^{-1}$  only observed in Fe doped ZnO thin film spectra, which is a good indication to recognize the

incorporation of individual dopant element. However, no IZO samples were reported in their work.

The changes in electrical properties of the IZO thin films with Zn content are portrayed in the work of Kim *et al.* (2008). The resistivity IZO thin films increases as the Zn content increases due to the combined effects of low carrier concentration and higher mobility values as observed in Figure 2.5. Socol *et al.* (2012) reported that the fabricated IZO thin film on PET substrate able to reach a minimum resistivity value of  $5.4 \times 10^{-4} \Omega \text{ cm}$ , comparable to the values reported on glass substrate.

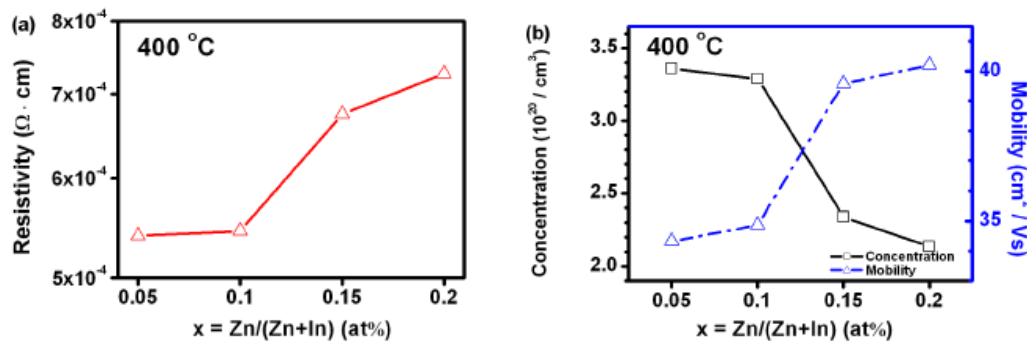


Figure 2.5. The resistivity, carrier concentration and mobility of IZO thin films dependence on Zn content. (Source: Kim *et al.*, 2008)

### 2.3 Characterization and properties of metal doped ZnO thin films by sputtering deposition

The films grown using sputtering is also sensitive to the deposition parameters. Hence, the properties of the thin film can be tailored by controlling the deposition parameters. Sputtering techniques have been widely used for thin film fabrication due to its abilities to produce a good quality film, not to mention having the advantage of better productivity when it comes to mass production (Kim *et al.*, 2007). Sputtering also have the advantage in providing multi-target deposition. Few papers on ZnO based thin films fabricated using sputtering techniques have been published since.

### **2.3.1 The effect of substrate temperature**

A few references have reported the dependence of the properties of ZnO based thin films deposited by sputtering method on substrate temperature. For un-doped ZnO thin films, Singh *et al.* (2007) investigate the effects of substrate temperature on samples deposited by DC magnetron sputtering. The ZnO thin film was deposited from room temperature (RT) until 600 °C, with a 100 °C step for each sample. The XRD spectra shows preferential c-axis of (0002) orientation with  $2\theta$  peak position ~34°. The peak positions of the (0002) are reported to have shifted from 34.18° of the ZnO deposited at room temperature to 34.44° for substrate temperature of 400 °C. The shift to higher angle when the substrate temperature increases is due to compressive lattice strain. The maximum compressive strain of  $8 \times 10^{-3}$  was calculated for the AZO thin film deposited at room temperature, which decreases nearly to zero for the AZO thin film with the substrate temperature of 400 °C. Hao *et al.* (2002) and Castro & Tavares (2015) explored the effects of substrate temperature on the properties of AZO and GZO thin films respectively. The AZO thin films, deposited on glass and polyimide (PI) substrates at temperature of 90 °C and 150 °C respectively, exhibit polycrystalline nature with (002) preferential orientation (Hao *et al.*, 2002). The (002) peak position do not shift with the increase of substrate temperature but become distinct and sharper due to improvement in crystal quality of the AZO thin film. This implies that the substrate temperature of 150 °C is better. The crystallite size of the AZO thin film deposited on glass substrate increases from 30 to 50 nm when the substrate temperature increases. For the PI substrate, the crystallite size changes from 17 to 40 nm. In the work of Castro & Tavares (2015), the XRD spectra of the GZO thin films exhibit the (002) diffraction peak with  $2\theta$  of 34.2°. Interestingly, the (002) peak position of the GZO thin film was slightly shifted to lower angle than the standard ZnO crystal of

34.4°. The shift in the angle is an indication of tensile stress acting along the c-axis of the thin film. From Bragg's law, the increase of the inter-planar spacing is due to the compressive stress build-up in the thin film, leading to the diffraction angle reduction. Jung *et al.* (2003) investigated the variation of DC magnetron sputtering parameters such as the O<sub>2</sub> flow rate, substrate temperatures, and deposition power on the properties of IZO thin films. The thin film was sputtered on glass and silicon wafer substrate using sintered IZO target. The XRD spectra of the IZO thin films with respect to substrate temperature ranging from room temperature up to 350 °C shows that all the IZO thin films were amorphous except for the thin film deposited at 350 °C. The IZO thin film deposited at 350°C shows a sharp peak of (222) orientation at  $2\theta = 30.5^\circ$ , indicating polycrystalline structure. The effect of the substrate temperature on the structural properties of the ZnO based thin films from different reports is summarized as in Table 2.2.

Table 2.2. Summary of the effect of substrate temperature on structural properties of ZnO based thin films by various references.

Thin film & substrate	Substrate temperature (°C)	Diffraction peak $2\theta$ (°)	Dominant orientation	Structure	Reference
IZO on glass	R.T 350	- 30.5	- (222)	Amorphous Polycrystalline	Jung <i>et al.</i> , 2003
ZnO on quartz	R.T 400	34.18 34.44	(0002) (0002)	Polycrystalline Polycrystalline	Singh <i>et al.</i> , 2007
AZO on glass and PI	90 (glass) 150 (glass) 90 (PI) 150 (PI)	34.10 34.24 34.18 34.24	(002) (002) (002) (002)	Polycrystalline Polycrystalline Polycrystalline Polycrystalline	Hao <i>et al.</i> , 2002
GZO on glass	270 290 300 310 320	34.20 34.20 34.20 34.20 34.20	(002) (002) (002) (002) (002)	Polycrystalline Polycrystalline Polycrystalline Polycrystalline Polycrystalline	Castro & Tavares, 2015

In an un-doped ZnO thin film at room temperature normally strong E<sub>2</sub> and weak A<sub>1</sub> (LO) modes was likely to appear in the backscattering geometry of the highly c-axis oriented ZnO film. The existence of LO modes is assigned to the zinc interstitial and oxygen defects. A small shoulder, sometimes observed at ~ 440 cm<sup>-1</sup> is associated with E<sub>2</sub> (high) mode. A weak presence of the E<sub>2</sub> (high) mode is an indication of structural defects. The emerging of the E<sub>2</sub> (high) modes was seen as the substrate temperature increases to 300 °C, in which coincides with better c-axis orientation of the film evident from XRD (Singh et al., 2007). At a substrate temperature of 600 °C, a distinct E<sub>2</sub> (high) mode with weak A<sub>1</sub> (LO) mode ~575 cm<sup>-1</sup> is observed.

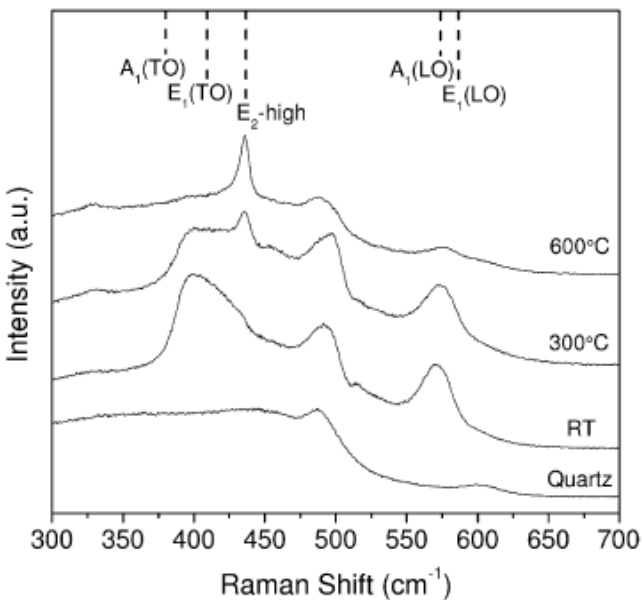


Figure 2.6. Raman spectra of ZnO thin films with various substrate temperature.  
(Source: Singh et al., 2007)

Charpentier *et al.* (2011) reported the influence of substrate temperature on AZO by means of Raman spectroscopy analysis. The AZO thin films were sputtered onto glass substrates from a ceramic ZnO target containing 1 wt. % Al<sub>2</sub>O<sub>3</sub>. The samples were deposited with different substrate temperature between RT until 325 °C. The

Raman spectra of the AZO thin films shows the domination of the A<sub>1</sub> (LO) mode at ~ 578 cm<sup>-1</sup> due to contribution of high and low wavenumber. The inset in Figure 2.7 of the AZO thin film Raman spectra shows the deconvolution of the broader A<sub>1</sub> (LO) peak into two peaks centered at 578 cm<sup>-1</sup> and 560 cm<sup>-1</sup> respectively. The broad Raman peak of 560 cm<sup>-1</sup> is associated with characteristic of a disordered phase while the narrow peak at 578 cm<sup>-1</sup> is attributed to the AZO crystallite. As the substrate temperature increases, the high wavenumber also increases compared to the low wavenumber indicating better crystallinity of the AZO thin films (Charpentier *et al.*, 2011). Additional peaks at 380 cm<sup>-1</sup> and 501 cm<sup>-1</sup> also observed in the Raman spectra. The peak that can be seen at 380 cm<sup>-1</sup> is attributed to the A<sub>1</sub> (TO) while the peak observed at 510 cm<sup>-1</sup> is due to the Al doping.

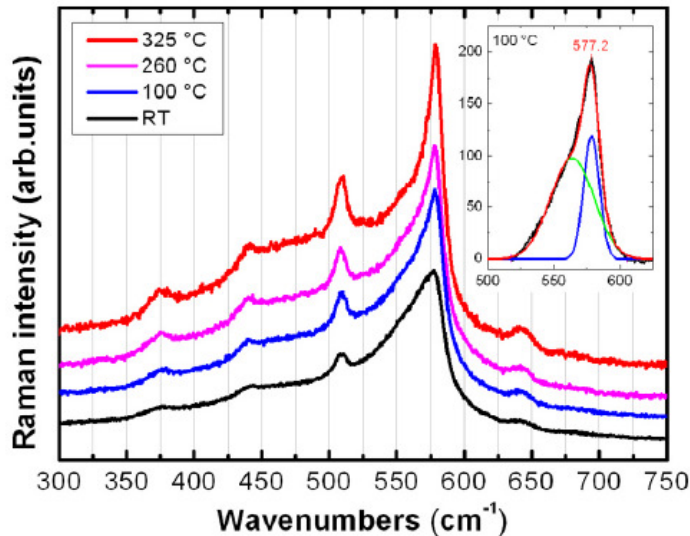


Figure 2.7. Raman spectra of AZO thin films sputtered at different substrate temperatures. (Source: Charpentier *et al.*, 2011)

An elevated substrate temperature seems to result in lower electrical resistivity. Binh *et al.* (2011) obtained the minimum resistivity value of  $1.79 \times 10^{-3} \Omega \text{ cm}$  for the IZO (2 wt. %) thin films deposited at 240 °C. At the temperature of 100 °C, the

resistivity obtained was  $138 \times 10^{-3} \Omega \text{ cm}$  (Binh et al., 2011). Nevertheless, the thin films with low resistivity is able to achieve at a relatively lower temperature, such as demonstrated in the work of Hao *et al.* (2002). The lowest resistivity was obtained for substrate temperature of 150 °C. Hao *et al.* (2002) produces AZO thin films with resistivity as low as  $8.5 \times 10^{-4} \Omega \text{ cm}$  and  $7.1 \times 10^{-4} \Omega \text{ cm}$  on PI and glass substrate respectively at substrate temperature of 150 °C. The challenge of using PI or organic substrate is that the higher substrate temperature of more than 150 °C tends to damage the substrate due to poor heat endurance. At low temperature, the sputtered ions does not acquire sufficient heat energy from the substrate, leading to bad thin film growth. Therefore, the optimum properties of AZO thin films with appropriate film growth are observed at a substrate temperature of 150 °C.

### 2.3.2 The effect of dopant content

The effect of dopant concentration or dopant content acting on the properties of the ZnO based thin films has been numerously reported. Different dopant elements may as well behave differently when doped into ZnO thin film, thus, affecting the structural, optical and electrical properties of the fabricated thin films. Binh *et al.* (2011), deposited IZO thin films with different In content ranging from 1 to 4 wt. % onto glass substrate to investigate the properties of IZO thin films. The changes in structural characteristics of the IZO thin film with the increasing In content are portrayed by the XRD spectra as in Figure 2.8. All samples show single (002) peak of the ZnO wurtzite structure with c-axis preferential growth. The crystallinity of the thin film were observed to degrade with the addition of In content evident from the decreasing (002) intensity peak.

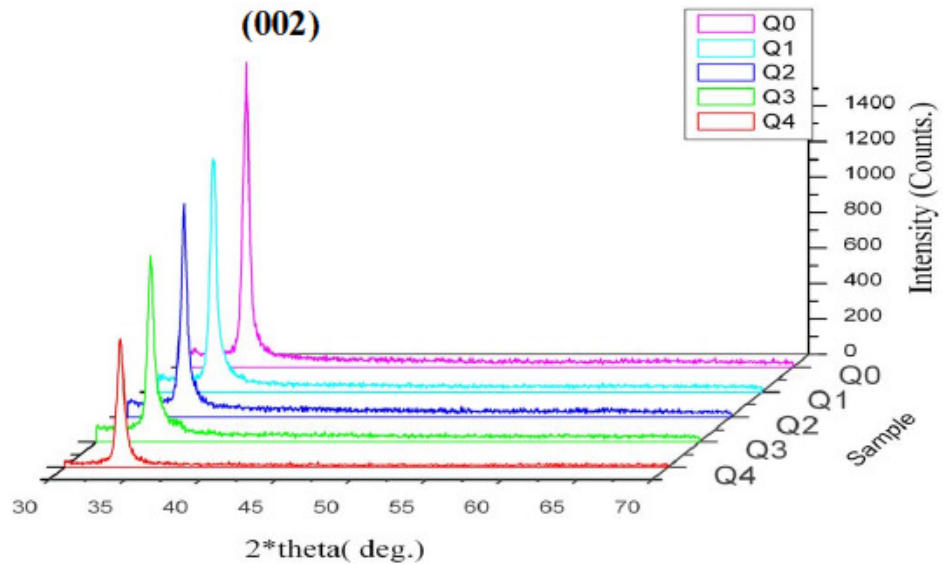


Figure 2.8. XRD spectra of the ZnO and IZO thin film in the range of 1 to 4 wt. % In. Q0 refers to un-doped ZnO, Q1 = 1 wt. % In, Q2= 2 wt. % In, Q3 = 3 wt. % In, and Q4 = 4 wt. % In. (Source: Binh *et al.*, 2011)

Lee *et al.* (2008) reported the effect of Ga content between the ranges of 2.27 to 10.81 wt. % on structural properties of GZO thin film. XRD spectra in Figure 2.9 shows preferred (002) plane for all samples, but the intensity was observed to continuously increase with the addition of Ga content reaching the maximum value at 6.65 wt. % Ga. Further addition of Ga content more than 6.65 wt. % decreased the intensity of (002) peak indicating crystallinity deterioration of the GZO thin films.

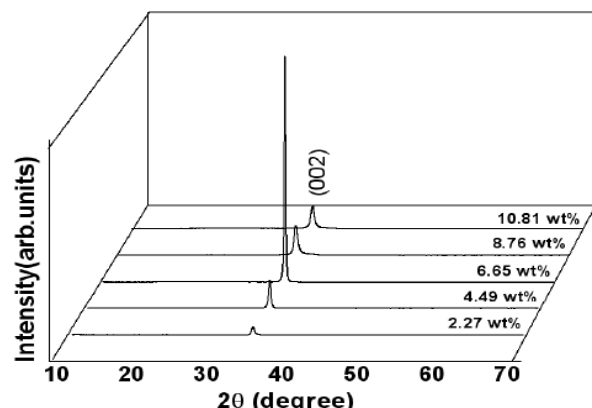


Figure 2.9. XRD spectra of GZO thin film with different Ga<sub>2</sub>O<sub>3</sub> wt. %. (Source: Lee *et al.*, 2008)

Generally, metal doped ZnO thin films have been reported to exhibit excellent optical transmittance within the visible region. ZnO thin film doped with various dopant are able to appear about 80 to 90% transparent in the visible region as evident from previous work summarized in Table 2.3.

Table 2.3. The average transparency in the visible wavelength of the ZnO thin films doped with various metal by references.

Thin film	Average transparency in the visible range	Reference
IZO	~ 90%	Binh <i>et al.</i> , 2011
IZO	~ 85%	Xie <i>et al.</i> , 2012
GZO	~ 80 – 85%	Lee <i>et al.</i> , 2008
GZO	~ 85%	Kim <i>et al.</i> , 2010
AZO	~ 80%	da Silva <i>et al.</i> , 2013

The changes of the ZnO thin films band gap with the increase of metal dopant content have been reported from previous studies. Xie *et al.* (2012) presented the shift in optical band gap of the un-doped ZnO thin film from 3.29 eV to 3.46 eV for the 5 at. % In sample. Further addition of the In content then reduces the value of the optical band gap. Similarly, in the work of Lee *et al.* (2008), the optical band gap of the un-doped ZnO increased from 3.37 eV to the maximum value of 3.61 eV at 6.65 wt. %  $\text{Ga}_2\text{O}_3$ . da Silva *et al.* (2013) reported that the addition of 0.5 wt. % Al into ZnO thin films widened the optical band gap from 3.28 eV for the un-doped ZnO to 3.36 eV. The broadening of the band gap when the dopant content increases is attributed to the increase of carrier concentration in the film. The term Burstein Moss shift is used to explain the widening of the band gap with the increase of carrier concentration due to metal dopant content. However, the widening of the band gap does not occur

continuously with further increase of metal dopant content. At the optimum dopant amount, the band gap of the thin film will reaches the maximum value. Further addition of metal dopant will reduce the band gap. The reduction of the band gap is associated with the formation of band tail states leading to band gap narrowing. The effect of dopant content on the electrical resistivity of doped ZnO thin film from the work of Binh *et al.*, 2011 and Lu *et al.*, 2006) is depicted in Table 2.4.

Table 2.4. Summary of electrical resistivity changes according to dopant content.

Dopant	Dopant content	Resistivity ( $\Omega$ cm)	References
In <sub>2</sub> O <sub>3</sub>	0 wt. %	$3.38 \times 10^{-3}$	Binh <i>et al.</i> , 2011
	1 wt. %	$3.00 \times 10^{-3}$	
	2 wt. %	$2.12 \times 10^{-3}$	
	3 wt. %	$2.17 \times 10^{-3}$	
	4 wt. %	$3.34 \times 10^{-3}$	
Al	0 at. %	70.7	Lu <i>et al.</i> , 2006
	1 at. %	$1.45 \times 10^{-3}$	
	4 at. %	$8.21 \times 10^{-4}$	
	7 at. %	$3.03 \times 10^{-3}$	
	10 at. %	$8.35 \times 10^{-2}$	

Both references are showing that the resistivity of the thin films reduces with the addition of dopant content reaching a minimum resistivity value before rising up again. Binh *et al.* (2011) attributed the initial decrease in the resistivity with the increasing In content is due to the increasing carrier concentration from In incorporation. Binh *et al.*, 2011 also discussed that the gradual increase of the resistivity when doped with